



This is a repository copy of *Orientation Control and Crystallization in a Soft Confined Phase Separated Block Copolymer*.

White Rose Research Online URL for this paper:
<http://eprints.whiterose.ac.uk/113045/>

Version: Accepted Version

Article:

Alharbe, L.G., Register, R.A. and Hobbs, J.K. (2017) Orientation Control and Crystallization in a Soft Confined Phase Separated Block Copolymer. *Macromolecules*, 50 (3). pp. 987-996. ISSN 0024-9297

<https://doi.org/10.1021/acs.macromol.6b02361>

This document is the Accepted Manuscript version of a Published Work that appeared in final form in *Macromolecules*, copyright © American Chemical Society after peer review and technical editing by the publisher. To access the final edited and published work see <https://doi.org/10.1021/acs.macromol.6b02361>

Reuse

Unless indicated otherwise, fulltext items are protected by copyright with all rights reserved. The copyright exception in section 29 of the Copyright, Designs and Patents Act 1988 allows the making of a single copy solely for the purpose of non-commercial research or private study within the limits of fair dealing. The publisher or other rights-holder may allow further reproduction and re-use of this version - refer to the White Rose Research Online record for this item. Where records identify the publisher as the copyright holder, users can verify any specific terms of use on the publisher's website.

Takedown

If you consider content in White Rose Research Online to be in breach of UK law, please notify us by emailing eprints@whiterose.ac.uk including the URL of the record and the reason for the withdrawal request.



eprints@whiterose.ac.uk
<https://eprints.whiterose.ac.uk/>

Orientation Control and Crystallization in a Soft Confined Phase Separated Block Copolymer

Lamiaa G. Alharbe,[†] Richard A. Register,[‡] Jamie K. Hobbs^{*,†}

[†]Department of Physics and Astronomy, University of Sheffield, Hicks Building, Sheffield,
S3 7RH, United Kingdom

[‡]*Department of Chemical and Biological Engineering and Princeton Institute for the Science and
Technology of Materials, Princeton University, Princeton, New Jersey 08544, United States*

***Corresponding author:**

Email address: Jamie.hobbs@sheffield.ac.uk

Phone: +44 (0)114 22 24532

Fax: +44 (0)114 22 23555

ABSTRACT

Microdomain orientation and crystallization were examined in a crystalline-amorphous diblock copolymer, hydrogenated poly (high-1,4-butadiene)-b-poly(high-3,4-isoprene) (E/MB), which forms cylinders of the crystallizable block (polyethylene, E). Atomic force microscopy (AFM) was used to locally control the orientation of the E cylinders. The orientation process and subsequent crystallization behavior were investigated in situ as a function of temperature by AFM. Fully confined crystallization was observed within the range of 25- 50 °C, with templated and breakout crystallization observed at higher crystallization temperature. The growth rate of templated crystallization along and perpendicular to the existing microdomain structure was measured and the ratio between these rates found to increase rapidly with decreasing temperature with a change from ~4.8 at 100 °C to ~8 at 97 °C. Two maxima in the degree of orientation of the crystallized regions were found, one at relatively small supercoolings (e.g. 95 °C) where the differential in growth rate along and across microdomain boundaries is high, and one at high supercoolings (25- 50 °C) where crystallization is completely dominated by nucleation.

Keywords: AFM; Block copolymer; Microdomain orientation control; Crystallization; In situ.

1. INTRODUCTION

Over the last six decades, extensive studies have been carried out to gain an understanding of the properties and behaviour of semi-crystalline polymers. In particular, crystallization in confinement has received great interest both experimentally¹⁻¹¹ and through simulation¹² in recent years. One reason for exploring confinement effects is that confined systems are becoming increasingly widespread, as devices and materials are constrained due to miniaturization. Secondly, the fundamental understanding obtained from studies of confinement length when it reaches an intrinsic length scale of the system can be extended to gain an understanding of crystallization in general.

Amongst the most convenient common methods to achieve confinement at the nanoscale are crystalline–amorphous diblock copolymers¹³ (with one crystallizable block), due to their self-assembled microdomains. Diblock copolymers generate various microphase separation structures¹⁴, such as spheres, cylinders, gyroids and lamellae. The shape, size and order of these microdomains can be controlled by varying the properties of the blocks (length, composition, affinity, etc.).

Controlling the orientation of the microdomains within a specific localized region is essential for the development of novel nanometre structures and in various applications¹⁵, such as data storage, lithography, computer memory and nanometre-scale templating¹⁶; if carefully controlled, the molecular orientation introduces anisotropy in the physical properties. Several approaches have been used to manipulate the orientation of copolymer microdomains, including electric fields^{17,18}, solvent fields¹⁹⁻²², chemically patterned substrates²³, thermal gradients²⁴, shear²⁵⁻²⁹, and AFM tips³⁰⁻³⁵.

AFM cantilever tips have been successfully used in the modification of a number of polymer thin films at the required resolution at the nanometre level. For example, the tip can be used

to scan or indent the films, creating ripple structures perpendicular to the fast scanning direction³⁶. The modification mechanism in this method is considered to be mechanical deformation^{30–33,37}.

AFM is a powerful technique for studying the crystallization of polymers, providing nanometre-scale information coupled with an ability to collect data in real time during the crystallization process³⁸. AFM has been successfully employed to study diblock copolymers^{39–41}, for example allowing direct visualization of crystallization in both cylindrical and spherical microdomains⁴².

In the current study, the AFM tip has been used to locally control the orientation of block copolymer microdomains before they crystallized, defining what direction the crystals initially grow relative to the blocks' interface. This simple process made the analysis of the impact of microdomain orientation on growth easier to determine. By controlling the orientation in a variable manner across the sample and then following the subsequent crystallization, complex structures with potentially interesting properties can also be formed.

2. EXPERIMENTAL METHODS

A hydrogenated poly (1,4-butadiene)-b-(3,4-isoprene) diblock copolymer, denoted as E/MB, was used. E is the hydrogenated high-1,4-poly butadiene (polyethylene), which is the crystallizable minority block, while MB is the rubbery amorphous majority block. The glass transition temperature (T_g) of the MB block is below room temperature ($-17\text{ }^\circ\text{C}$). The molar masses of the E and MB blocks were 17 and 45 kg/mol, respectively. The volume fraction for E, f_E , is 0.27, which results in a cylindrical mesophase of polyethylene in the phase separated state. The synthesis and characterization of this E/MB diblock has been described in detail previously².

The samples were prepared by melt casting onto a glass coverslip at 130 °C (above the melting point) using a Linkam TP94 hot stage. Then, they were thinned by a razor blade, producing films with a thickness of few micrometers. The films were then quenched to the examined crystallization temperature (in the range of 94–115 °C) at the maximum cooling rate of the hot stage, nominally 90 °C/min.

AFM was performed in tapping mode, using a Veeco Dimension 3100 AFM with a Nanoscope IIIA controller. Silicon tapping cantilevers (nominal spring constant 40 Nm⁻¹ and resonance frequency ~ 300 kHz) were used (TESPA-V2). All images were taken at 512×512 pixels. The majority of the images were phase images in which the contrast contains a mixture of the adhesive and mechanical properties of the film surface.

The experimental setup is shown in **Figure 1a**. Once the films had been prepared on the substrate, they were placed on a heater at a temperature range from 110–120 °C (Below 110 °C, the tip induced crystallization as presented in **SI1**).

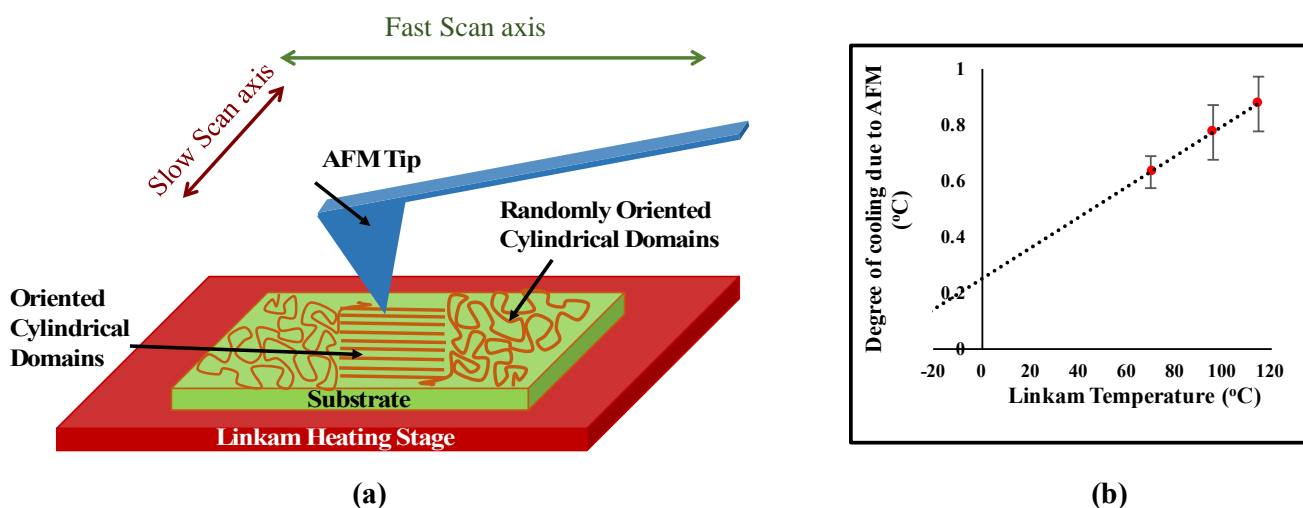


Figure 1: (a) Schematic diagram of experimental setup. The E/MB microdomains are randomly oriented initially. The AFM tip orients the E/MB microdomains in its fast scan direction while a Linkam heating stage heats the film above the melting point (i.e. 115 °C). (b) Calibration plot showing the correction that should be applied to the Linkam TP94 temperature displayed in order to

acquire the actual sample temperature. The cooling effect of the AFM tip on sample temperatures was measured between approximately 70 °C and 115 °C. Error bars are the standard deviations from several measurements. As the measured temperature corrections are less than 1 °C the ‘as displayed’ temperatures are given in this paper.

Following an initial imaging scan the sample was imaged with high force over the area to be oriented, using a setpoint of 0.2-0.4 V compared to a free amplitude (i.e. amplitude when off the surface) of ~3 V (i.e. a relative setpoint, r_{sp} , of ~0.1), corresponding to an rms amplitude of ~1.8-3.5 nm and ~27 nm respectively. Using the approach outlined in ⁴³ this equates to a force of approximately 3.7 nN. The average bending of the cantilever when carrying out this low amplitude imaging was 0.09 nm, corresponding to a force of approximately 3.8 nN (assuming the nominal spring constant for the cantilevers used), in good agreement with the theoretical estimate. The area was then re-imaged at low force ($r_{sp} \sim 0.8$), to determine the impact of the orienting scan. Following this orientation procedure the sample was then cooled on the Linkam to the desired temperature with the tip retracted from the surface, and then imaged in situ during subsequent crystallization.

Due to the temperature variation between the unheated AFM tip and the sample the temperature of the sample area being scanned will deviate from that which is set on the heater. Therefore, a calibration was done to account for this cooling effect of the AFM tip. The calibration was performed using materials with well-defined melting point transitions (see **Figure 1b**). All the temperatures in this paper are the heater displayed temperature as the difference between them and the actual temperatures is less than 1 °C.

3. RESULTS AND DISCUSSION

This work can be split into two main sections: the first considers controlling the orientation of microdomains by the AFM tip and the second, the crystallization behaviour as a function of temperature.

3.1. Alignment of E/MB microdomains by the AFM tip

3.1.1. Orientation Control of Microdomains

The AFM tip was used as a tool to orient the crystalline cylindrical domains mechanically in its scanning direction before they crystallized. After aligning the cylinders of the E/MB, the subsequent crystallization behaviour was examined in situ at different temperatures.

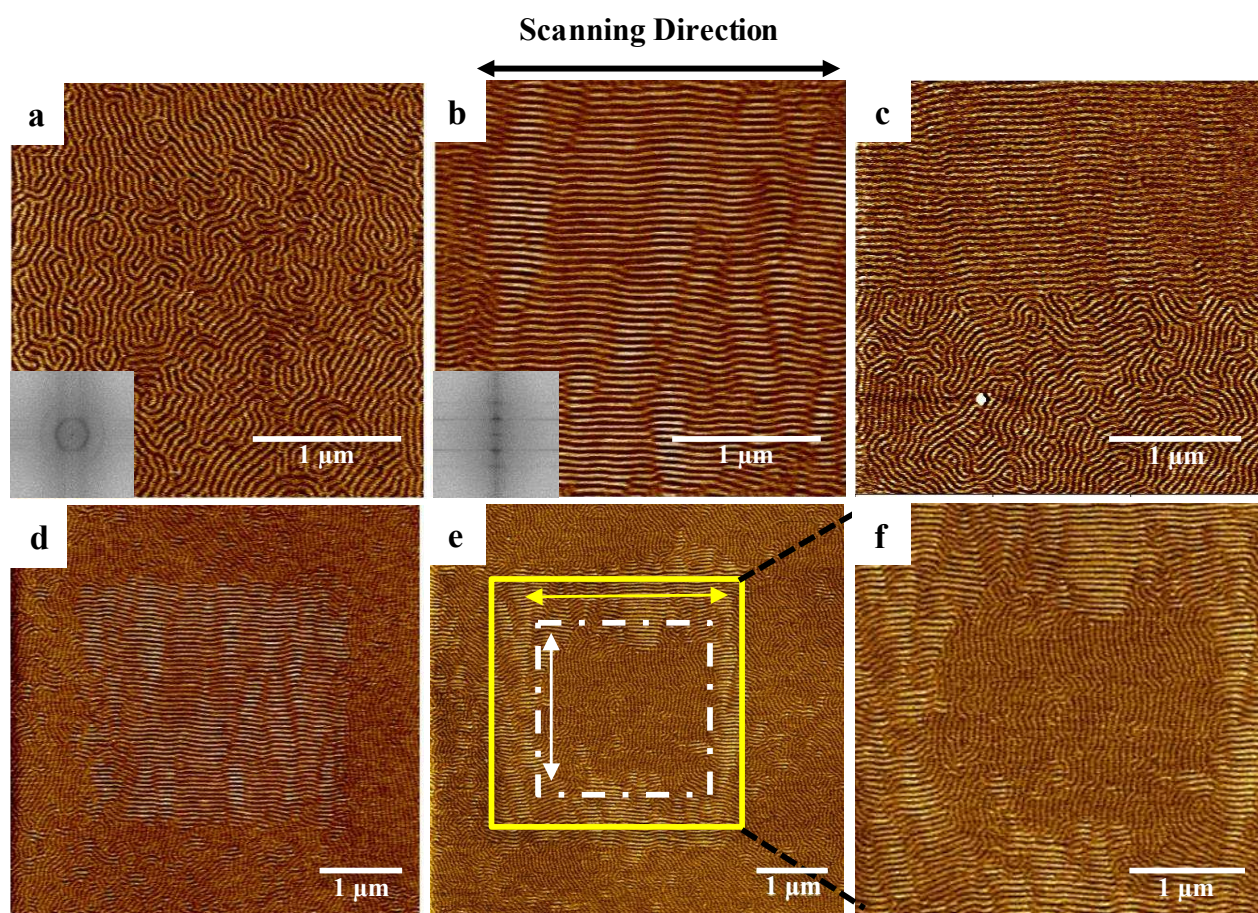


Figure 2: AFM phase images showing: (a) the natural random orientation of E/MB microdomains in the melt state, (b) the cylindrical microdomains oriented by the AFM tip, (c) the boundary between random and oriented cylinders, and (d) the oriented cylindrical microdomains in a matrix of random

domains. The insets in **(a)** and **(b)** are the corresponding Fast Fourier Transform patterns of the cylindrical microdomains showing essentially random orientation in **(a)** and a high degree of orientation in **(b)**. **(e)** AFM phase image showing aligned cylinders of E/MB in two different directions according to the AFM tip scanning direction. The arrows indicate the fast scanning direction in the two differently oriented regions (white and yellow squares). Image **(f)** is a magnified view of the yellow square region in image **(e)**. Colour scales are **(a-b)** 5°, **(c)** 3°, **(d)** 5°, and **(e-f)** 4°.

Figure 2(a) illustrates an AFM phase image of the melt microdomain structure in E/MB. The cylindrical microdomains that resulted from the initial film preparation were oriented randomly with cylinders largely lying in the plane of the surface. **Figure 2(b)** shows the aligned cylindrical microdomains resulting from scanning of the AFM tip over the film surface, at low relative setpoint.

The FFTs of the AFM images show the disorder, **(a)**, and high degree of order, **(b)**, of the cylindrical microdomains. **Figures 2(c)** and **(d)** show further examples. A clear boundary between the oriented domains (in the top half) and the random domains (in the bottom half) can be seen in image **(c)**. Image **(d)** illustrates the aligned cylindrical microdomains in a matrix of random cylinders.

The alignment direction of the cylindrical microdomains can be controlled by altering the tip travel direction. **Figure 2 (e)** shows an example resulting from multiple tip scans having been carried out on the sample. The tip first scanned parallel over a 4×4 μm area (the yellow square in image **(e)**), aligning the random cylindrical microdomains along its scanning direction. Subsequently, the tip was scanned perpendicularly to the initial scan direction over a 2.5×2.5 μm area (the white square in image **(e)**) in the approximate centre of the previously aligned microdomains, resulting in reorienting this area orthogonally to the previously aligned area in the matrix of a random region (image **(e)**). We note that orientation at the

boundary between the two oriented regions is less clearly defined than that between oriented and disoriented areas, implying a greater barrier to the reorientation process.

3.1.2. Enhanced Microdomain Ordering

The AFM tip is able to align cylindrical microdomains in its scanning direction, although in some cases defects—dislocations, sometimes clustered together— were observed (**Figure 3**).

We explored the extent to which multiple scans impacted upon the number of defects.

Scanning the same area more than once (with the same hard tapping force conditions initially used for alignment, low amplitude and low relative set-point $r_{sp} \approx 0.1$) reduced the number of defects. Accordingly, areas that were scanned once contained a greater number of defects per unit area compared with areas scanned more than once. This situation is shown in **Figure 3**. The cylindrical microdomains are highlighted, from which it can be seen that the number of defects was reduced by simply increasing the number of scans with the same hard tapping conditions.

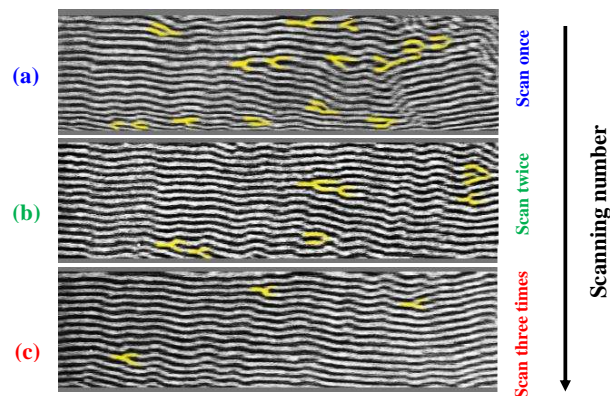


Figure 3: AFM phase images showing the effect of scanning number on the defects per unit area, **a-c** 1st, 2nd and 3rd scans, respectively, with relatively high tapping force (low amplitude and low $r_{sp} \approx 0.1$) at 115°C. The defects are highlighted in yellow to aid the reader in following the reduction in defects as a function of the number of scans. The image size is $3 \times 0.75 \mu\text{m}$ and the black-to-white scale is 7°.

On the other hand, there were a few cases where some defects were formed by increasing the number of scans (see **SI2**). Nevertheless, in those cases, the number of defects per unit area was reduced by increasing the number of scans over the film, resulting in better ordering in general. **Figure 4** is a plot showing this result from several experiments. The change in the number of defects was found to vary with the number of scans but was approximately linear, with an overall average decrease in the number of defects per square micrometre of 0.9 per scan.

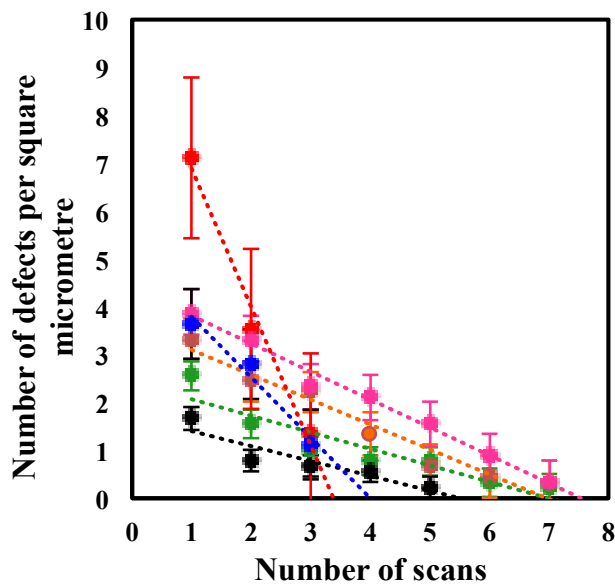


Figure 4: A plot showing the number of defects as a function of the number of scans (each colour indicates an independent experiment). Error bars are the standard errors.

Having formed oriented domains of cylinders we now study the impact of orientation on subsequent crystallization.

3.2. Crystal Morphology as a Function of Temperature

a) Morphology Formation from Unoriented Cylindrical Microdomains

The morphology formed depends on the temperature of crystallization. Therefore, in order to see the effects of temperature on the structure of the crystals formed, the same sample was isothermally crystallized at different temperatures. The sample was transferred very quickly from the heating stage held at 130 °C to another heating stage placed under the AFM and held at the crystallization temperature for several minutes, allowing the sample to crystallize. The duration of holding the sample at the specific temperature depended on the crystallization rate, e.g. crystallization at 50 °C took place very fast so at this temperature the sample was held for 5 minutes to ensure complete crystallization, however at higher temperatures, crystallization occurs slower, needing more time to be completed. An example is shown in **Figure 5**. The same sample was used to investigate both the effects of temperature on the structure of the crystals formed and the temperature at which the crystals would be completely confined within the microdomain melt structure. The order that these experiments were performed in was first at room temperature, then 50 °C, 60 °C, 70 °C, 80 °C and finally 100 °C.

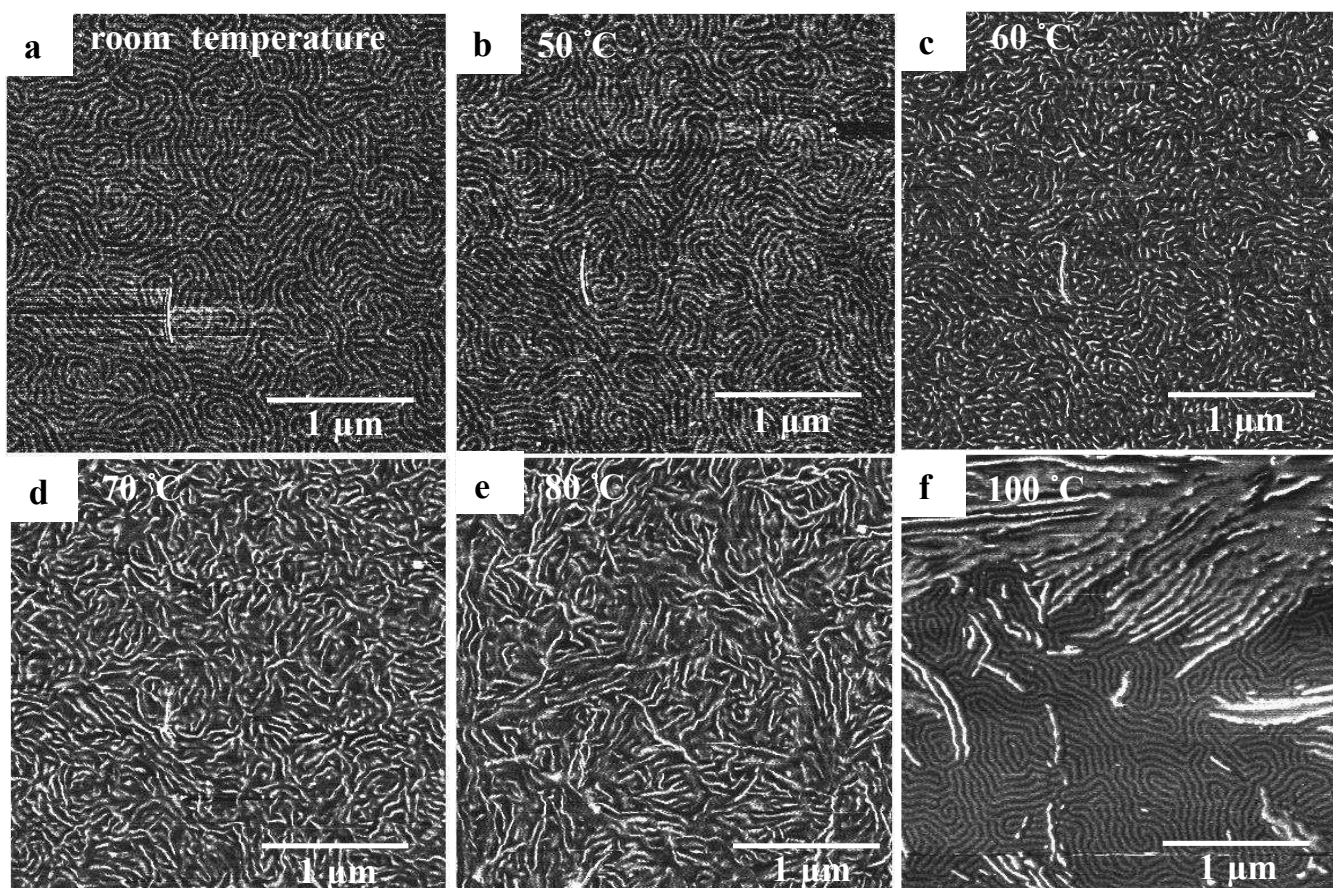


Figure 5: AFM phase images of crystallized E/MB after isothermal crystallization (the same area) at: (a) room temperature, (b) 50 °C, (c) 60 °C, (d) 70 °C, (e) 80 °C and (f) 100 °C (unoriented cylinders). These images are cropped from the larger images shown in Figure S3a. Colour scales are (a) 9°, (b) 8° (c-d) 11°, and (f) 7°.

Figure 5 shows images of different crystal morphologies formed isothermally at a range of temperatures: room temperature, 50 °C, 60 °C, 70 °C, 80 °C, and 100 °C. In general, confined crystallization can be observed in two cases: firstly when the T_c of the crystalline block (E, in this study) is lower than the T_g of the amorphous block (MB in this study) and secondly when both the crystalline and amorphous blocks are strongly segregated in the molten state and the degree of crystallinity is relatively low³. Although here in all cases the $T_{c,E}$ was greater than $T_{g,MB}$ for the studied system, a range of crystallization modes was observed. At temperatures of 50 °C and below, the crystals were fully confined by the pre-existing cylinder microdomains. However, at temperatures higher than 50 °C, templated

crystallization (i.e. where the crystals generally grow parallel to the axes of the cylindrical microdomains, but not exclusively) was observed. At 100°C, breakout crystallization is observed, with the initially cylinder shaped crystals widening to form lamellae. Note the vertical line in the centre of the images is a defect in the film that was used to help return to the same place each time.

Moreover, by comparing the change in surface morphology caused by E crystallization at different temperatures, it is clear that the nucleation density quickly increases as the crystallization temperature lowers. At low supercoolings (high temperatures), such as 100 °C, very few nucleation sites were found, as seen in **Figure 5 (a)**. However, at larger supercooling (low temperatures), such as 80 °C and 70 °C, there was a significant increase in the density of nucleation sites.

The above work was carried out on un-oriented microdomains. The same approach was used to investigate the dependence of morphology formed from oriented microdomains on the temperature of crystallization (**Figure 6**). Similar results were obtained.

b) Morphology Formation from Oriented Cylindrical Microdomains

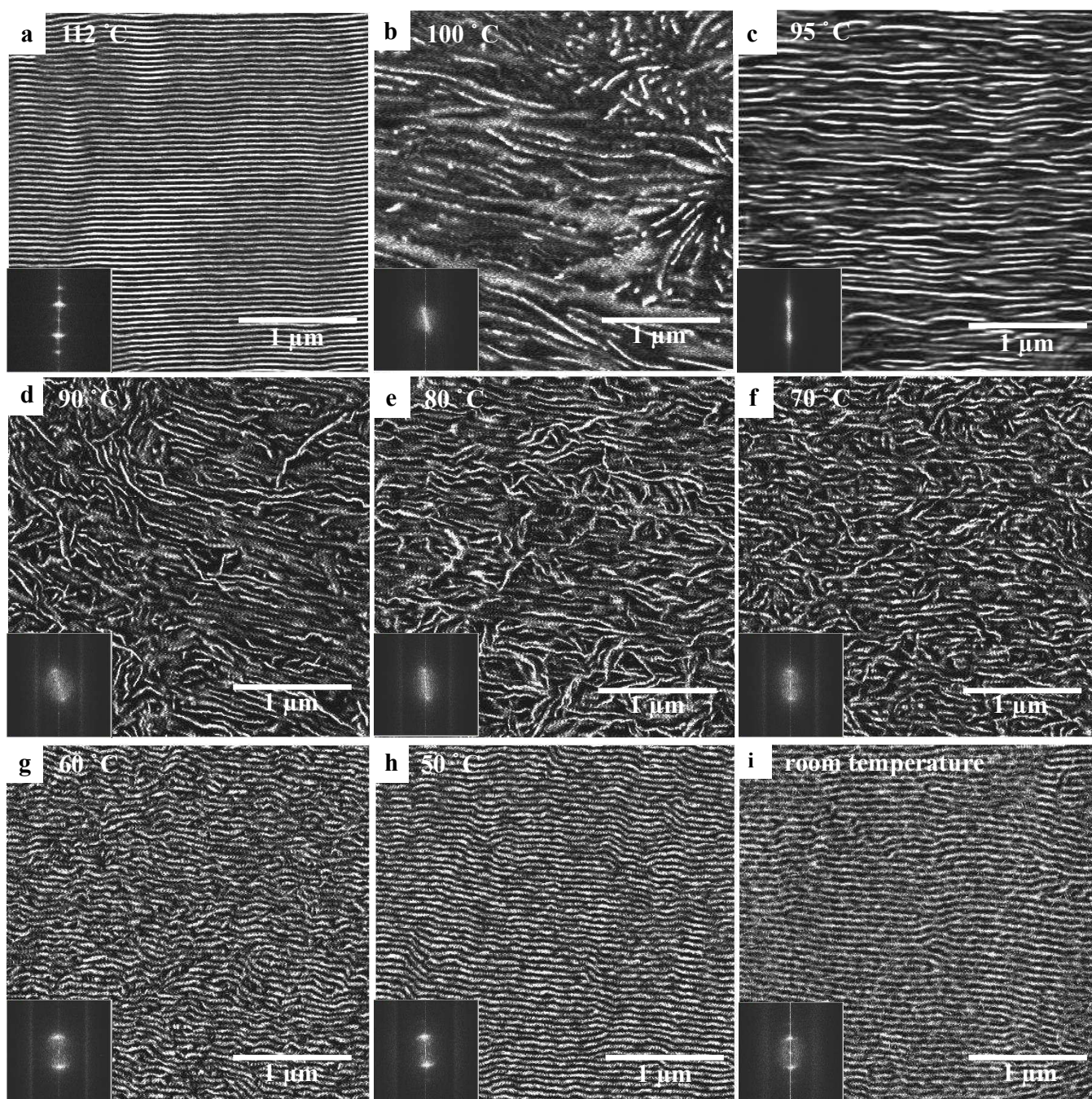


Figure 6: AFM phase images of E/MB showing (a) an orientated melt structure at 112 °C and images (b-i) showing crystallized E/MB after isothermal crystallization at: (b) 100 °C, (c) 95 °C, (d) 90 °C, (e) 80 °C, (f) 70 °C, (g) 60 °C, (h) 50 °C and (i) room temperature. The insets are 2D fast Fourier

transforms of the images. Colour scales are (a) 8°, (b) 7°, (c) 8°, (d) 9°, (e-f) 10°, (g) 11°, and (h-i) 12°.

Figure 6 shows the melt structure of the oriented E/MB at 112 °C in image (a), and the fully crystallized film after quenching to room temperature in image (i). The crystals were strictly confined within the melt structure at room temperature.

The change in crystal orientation with temperature is striking, with an initial increase in orientation on cooling, lower orientation at moderate supercooling e.g. at 80 °C and then increased orientation at high supercooling. To explore this further we follow the crystallization process in situ.

An equivalent set of data for samples that had not been pre-oriented is shown in **Figure S3b**.

3.3. Following Crystallization in Pre-Oriented Domains in Situ

After aligning the cylindrical microdomains in the melt phase with the AFM tip, the film was then cooled to the desired crystallization temperature to be isothermally crystallized in order to investigate the subsequent crystallization.

3.3.1. Crystallization Behaviours at Different Temperatures

The crystallization behaviour was investigated by observing the crystallization process in real time at various temperatures. **Figure 7** shows an example of following crystallization at 95 °C. Another example, at 99 °C, is given in **SI4**. The crystallization was followed in the temperature range of 95–101 °C, where the AFM was able to image the crystallization in situ, in order to study the influence of temperature on crystallization. Below 95 °C, it was not possible to follow the crystal growth in real time, as the crystallization was found to be complete before the imaging could be carried out. Above 101 °C, no crystallization was observed over several hours of experiment.

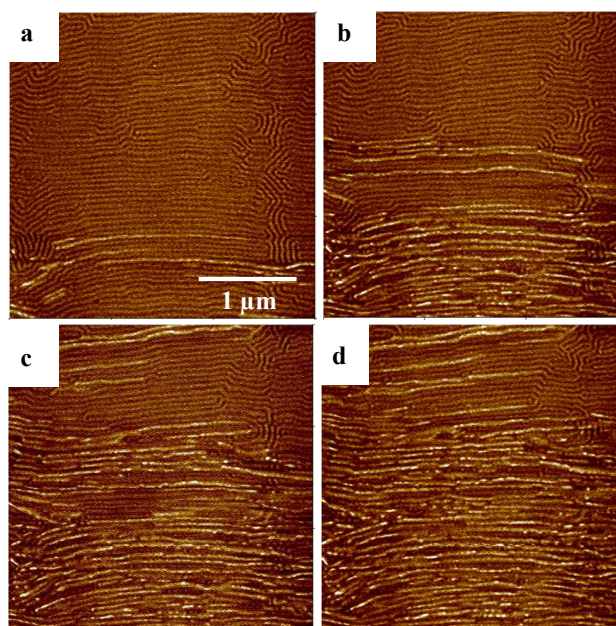


Figure 7: A sequence of AFM phase images collected at 95 °C showing the crystallization in E/MB from the aligned melt structure. Colour scale represents a change in phase of 5°.

Figure 7 shows templated crystallization occurring at 95 °C, with the polyethylene crystals generally following the contours of the pre-existing E cylinders in the melt. At 99 °C (**SI4**), some regions of breakout crystallization could also be observed, as previously documented for this polymer⁴⁴.

In combined in-situ and ex-situ images we found interesting behaviour of crystals at a different range of temperatures that can be divided into four categories. First, at very high temperature (e.g. 100 °C) crystals cross domain boundaries easily which leads to breakout; in some regions, instead of the needle-like crystals present within cylindrical microdomains, flat lamellae lying in the plane of the sample surface can be observed. Second, as the temperature was reduced (e.g. 95 °C) crystals grow much faster along the microdomains leading to templated crystallization, and the flat lamellae resulting from breakout are not generally observed. Third, as temperature was reduced further (e.g. 80 °C) crystals are observed to cross domain boundaries again, because the nucleation density increases and the distance

between nuclei, required for the growing crystals to reorient, is reduced. Finally, as the temperature is reduced even further (e.g. 50 °C), crystallization becomes confined within the microdomains. It is unclear whether this is due to confinement changing growth direction or because the nucleation density is so high that it dominates over growth, but the latter seems most likely. Formation of lamellae has only been observed at high temperatures (e.g. 100 °C) where the crystals widen and break out the cylindrical microdomains, while at lower temperatures only needle-like crystals within cylindrical microdomains have been observed. In these studies of isothermal crystallization (i.e. not quenching to room temperature) the best orientation obtained was at 95 °C. If our hypothesis— that it is nucleation that is dominating at the lowest temperatures— is correct, then although the crystal domains are oriented at these low temperatures, we would not expect the crystal lattice to be oriented, while at 95 °C where it has grown along the orientation direction we would expect both the domain and the lattice to have a common orientation. We have not been able to test this due to the relatively small size of the oriented regions in our samples.

3.3.2. Growth Rate

The growth rate of crystals was studied as a function of temperature to obtain quantitative kinetic information about the crystallization behaviour. The distance of the crystal growth was measured in a succession of images by measuring how far the growth front of the crystal moved from one image to the next. The average growth rates of a number of crystallites growing parallel to the cylinder axes, as well as those growing perpendicular, at temperatures of 97–100 °C were measured and compared.

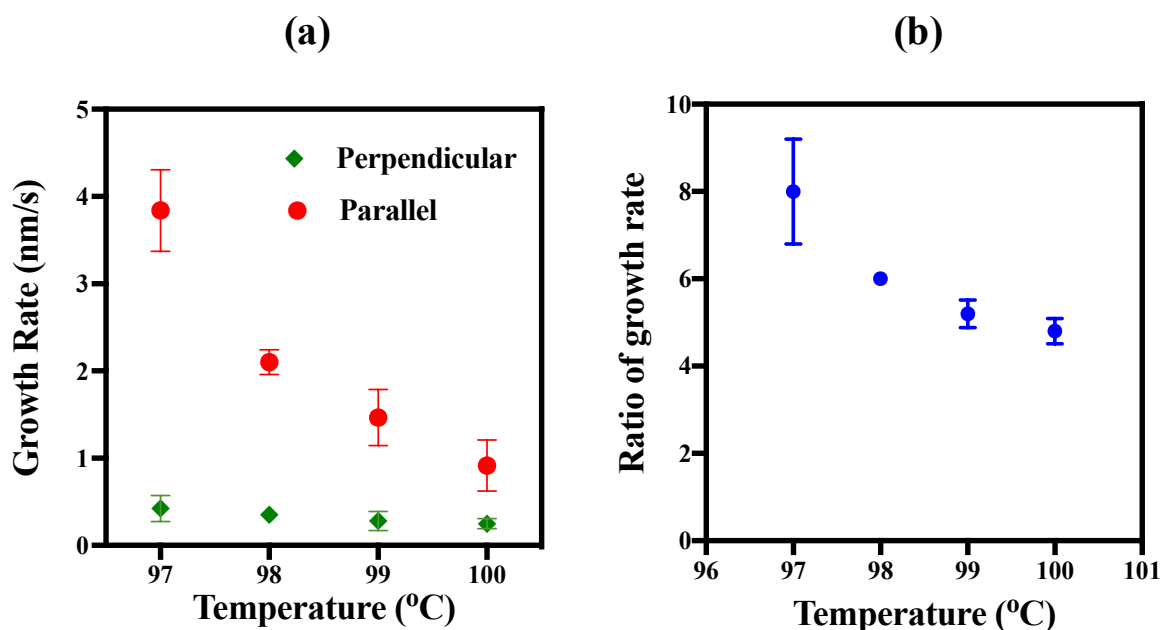


Figure 8: Graphs showing the relationship between temperature and (a) the average growth rates along the cylinder axis and the growth rate perpendicular to the cylinder axis and (b) the ratio of the two.

From **Figure 8 (a)** it can be clearly seen that the growth rates along cylinders are much higher than the growth rates perpendicular to them. Moreover, as the temperature increased, the growth rate ratio of the crystals growing along the cylinders compared to those growing against them decreased sharply from ~ 8 at $97\text{ }^{\circ}\text{C}$ to ~ 4.8 at $100\text{ }^{\circ}\text{C}$ as shown in **Figure 8 (b)** (see the corresponding values of these graphs in **SI 5**). Hence, two outcomes were observed related to increasing the crystallization temperature: a decrease in the overall crystallization rate and a decrease in the relative difference between the growth rates along the cylinders and against them.

These data imply that, at high temperatures, an increase in the diffusion of E blocks between domains and a decrease in the rate of take-up of E chains onto the growth front combine to decrease the difference in growth rates along and against the cylinders, since the time for a

chain to diffuse from one cylinder to another becomes comparable to the time required for a chain to add to the growing crystal, and breakout crystallization can occur.

3.3.3. The Transition from 'Breakout' to 'Templated' Growth

At low supercooling the nucleation density is low so for crystals to grow relatively straight in un-oriented areas they must cross domain boundaries. Growth parallel to the oriented microdomains happens through re-orientation of the growth direction, either from bending or crystal branching. Such a process is shown in **Figure 9**.

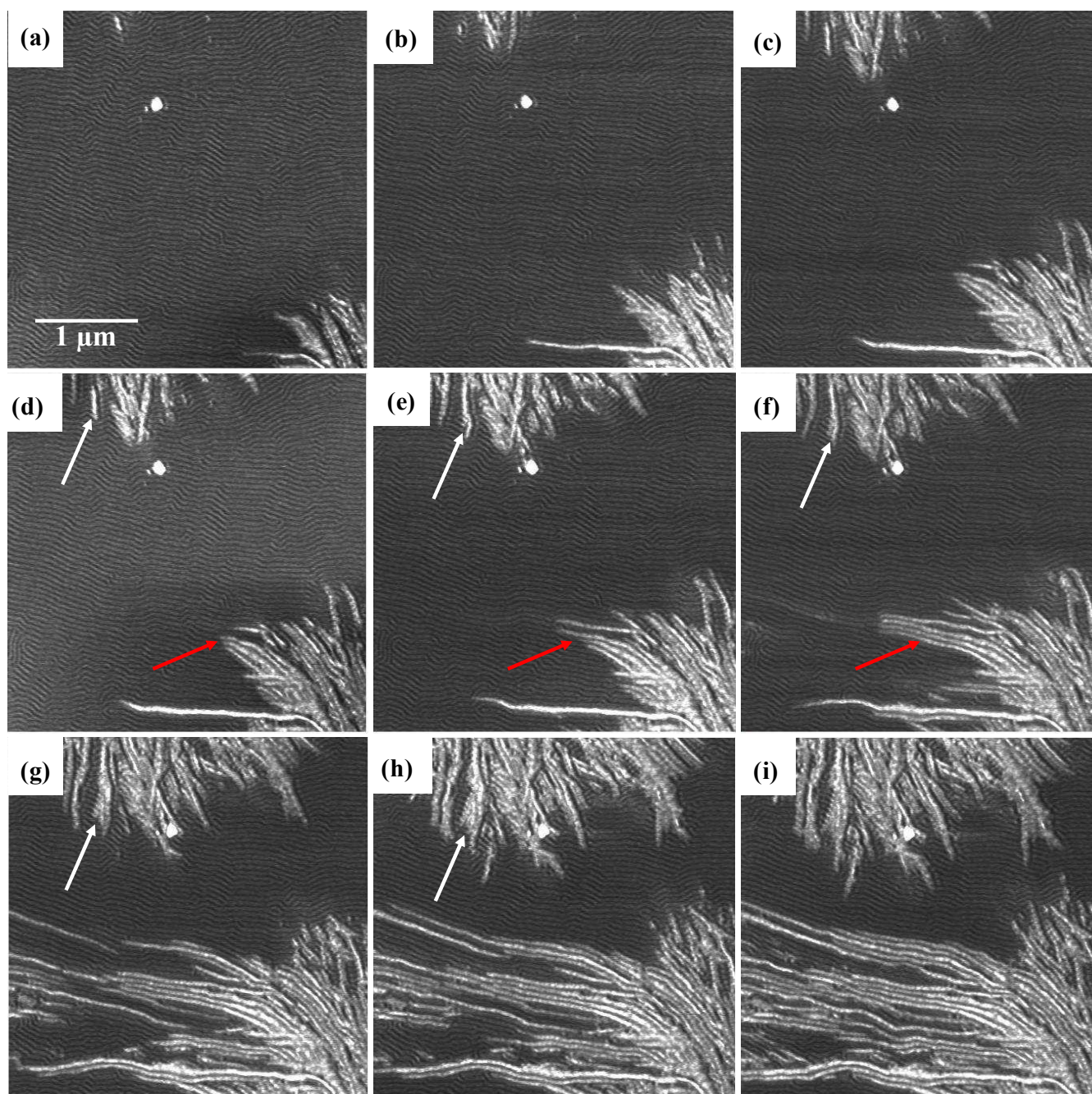


Figure 9: In situ AFM phase images showing E/MB crystallization at 101 °C. Each image was captured in 128 s, and the image scan size is 3.5 μm . Arrows have been added to aid the reader in following the branching and curving of crystals growing against the melt structure. Black to white scale 6°. These images are cropped from the larger images shown in **SI6**. The full series with some corresponding height images is presented in **SI6**.

Figure 9 shows the partial branching of crystals that are growing against the melt microdomains. Two different behaviours for the branching crystals are illustrated:

- a) Crystal thickening and branching (see white arrows in **Figure 9(d-h)**) until it meets another crystal (**SI6**).
- b) Crystals adjust their growth directions to be along the existing melt cylinders with an increase in their growth rate, without any branching (the red arrow in **Figure 9(d-f)** indicates such a situation).

Crystals growing parallel to the cylinder axes show very low rates of branching compared with crystals growing perpendicular to the cylinders. In the case of crystals growing parallel to the cylinder axes, the crystallization front is always surrounded to the sides by uncrystallisable material. To branch into another domain would require a significant alteration of the local melt structure by diffusion of copolymer. As this diffusive process is slow relative to the growth of the crystal along the cylinder, it becomes unlikely that diffusive processes will have enough time to alter the domain structure at the growth front to form branches before the bulk of the material is consumed by the crystallization along the melt domain. In the case of crystals growing against the melt domain, the crystal front is constantly being forced to reorganize the local melt structure in order to grow. Under these conditions, crystal growth is slowed significantly, enabling effects such as the branching and thickening of the crystals to occur.

4. CONCLUSION

The crystallization behaviour of a cylinder-forming E/MB diblock copolymer has been investigated in real time, in situ combined with ex situ imaging by AFM. The AFM tip has been successfully used to control the orientation of the cylindrical E microdomains in

different directions according to its scan direction, and then following the subsequent crystallization. It was found that the number of defects (dislocations) reduced with an increase in the number of orienting scans. Depending on the thermal conditions examined, a change from fully confined crystallization to templated and breakout crystallization was observed. Confined behaviour of crystals was observed at very high supercooling (room temperature and 50°C), templated crystallization at intermediate temperatures, and a mixture of templated and breakout crystallization at the highest temperatures, e.g. at 100 °C. The difference in the morphology and the behavior of crystals growing parallel to the axes of the pre-existing melt cylinders, and those growing perpendicular, has been explored. The growth rates of confined crystals were higher than those of crystals growing against the established melt structure. As the crystallization temperature increased, the overall crystallization rate and the relative difference between the growth rates along the cylindrical microdomains and against them decreased. This indicates that small variations in crystallization temperature can have significant effect on the morphology and properties particularly where the melt has been pre-aligned as may well happen during processing.

ASSOCIATED CONTENT

Supporting Information:

AFM images showing crystallization induced by the AFM tip. AFM images showing reduction in numbers of defects. AFM images showing crystal morphology as a function of temperature. AFM images showing crystallization in pre-oriented domains and a movie of the same data. A table showing growth rates as a function of temperature parallel and perpendicular to orientation axis.

NOTES

The authors declare no competing financial interest.

ACKNOWLEDGMENTS

We would like to thank Dr. Nicholas Mullin for his support and the Ministry of Higher Education in Saudi Arabia for funding. R.A.R. gratefully acknowledges support from the National Science Foundation, Polymers Program (DMR-1402180). The authors thank Drs. Gary Marchand (Dow Chemical) and Daniel Quiram (Princeton University) for the synthesis of the E/MB diblock copolymer.

REFERENCES

- (1) Loo, Y. L.; Register, R. A.; Ryan, A. J. Polymer Crystallization in 25-nm Spheres, *Phys. Rev. Lett.* **2000**, 84, 4120–4123.
- (2) Quiram, D. J.; Register, R. A.; Marchand, G.R. Crystallization of Asymmetric Diblock Copolymers from Microphase-Separated Melts, *Macromolecules* **1997**, 30, 4551–4558.
- (3) Zhu, L.; Chen, Y.; Zhang, A. Q.; Calhoun, B. H.; Chun, M. S.; Quirk, R. P.; Cheng, S. Z. D.; Hsiao, B. S.; Yeh, F. J.; Hashimoto, T. Phase Structures and Morphologies Determined by Competitions among Self-Organization, Crystallization, and Vitrification in a Disordered Poly(ethylene oxide)-b-polystyrene Diblock Copolymer, *Phys. Rev* **1999**, 60, 10022–10031.
- (4) Zhu, L.; Cheng, S. Z. D.; Calhoun, B. H.; Ge, Q.; Quirk, R. P.; Thomas, E. L.; Hsiao, B. S.; Yeh, F.; Lotz, B. Crystallization Temperature-Dependent Crystal Orientations

- within Nanoscale Confined Lamellae of a Self-Assembled Crystalline - Amorphous Diblock Copolymer, *J. Am. Chem. Soc.* **2000**, 122, 5957–5967.
- (5) Huang, P.; Zhu, L.; Cheng, S. Z. D.; Ge, Q.; Quirk, R. P.; Thomas, E. L.; Lotz, B.; Hsiao, B. S.; Liu, L.; Yeh, F. Crystal Orientation Changes in Two-Dimensionally Confined Nanocylinders in a Poly(ethylene oxide)-b-polystyrene/Polystyrene Blend, *Macromolecules* **2001**, 34, 6649–6657.
- (6) Opitz, R.; Lambreva, D. M.; De Jeu, W. H. Confined Crystallization of Ethylene oxide-butadiene Diblock Copolymers in Lamellar Films, *Macromolecules* **2002**, 35, 6930–6936.
- (7) Gao, W.-P.; Bai, Y.; Chen, E.-Q.; Zhou, Q.-F. Crystallization and Melting of poly(ethylene oxide) Confined in Nanostructured Particles with Cross-Linked Shells of Polybutadiene, *Chinese J. Polym. Sci.* **2005**, 23, 275–284.
- (8) Zhu, L.; Mimnaugh, B. R.; Ge, Q.; Quirk, R. P.; Cheng, S. Z.; Thomas, E. L.; Lotz, B.; Hsiao, B. S.; Yeh, F.; Liu, L. Hard and Soft Confinement Effects on Polymer Crystallization in Microphase Separated Cylinder-Forming PEO-b-PS/PS Blends, *Polymer* **2001**, 42, 9121–9131.
- (9) Xu, J.-T.; Zhao, Y.-Q.; Liang, G.-D.; Fan, Z.-Q. Melting–Recrystallization of Block Copolymer Crystals in Confined Environments, *Polym. J.* **2005**, 37, 43–46.
- (10) Loo, Y. L.; Register, R. A.; Ryan, A. J.; Dee, G. T. Polymer Crystallization Confined in One, Two, or Three Dimensions, *Macromolecules* **2001**, 34, 8968–8977.
- (11) Hamley, I. W.; Fairclough, J. P. A.; Ryan, A. J.; Bates, F. S.; Towns-Andrews, E. Crystallization of Nanoscale-Confined Diblock Copolymer Chains, *Polymer* **1996**, 37, 4425–4429.

- (12) Zha, L.; Hu, W. Molecular Simulations of Confined Crystallization in the Microdomains of Diblock Copolymers, *Progress in Polymer Science* **2016**, 54, 232-258.
- (13) Zhu, L.; Cheng, S. Z. D.; Calhoun, B. H.; Ge, Q.; Quirk, R. P.; Thomas, E. L.; Hsiao, B. S.; Yeh, F.; Lotz, B. Phase Structures and Morphologies Determined by Self-Organization, Vitrification, and Crystallization: Confined Crystallization in an Ordered Lamellar Phase of PEO-*b*-PS Diblock Copolymer, *Polymer* **2001**, 42, 5829–5839.
- (14) Bates F. S.; Fredrickson, G. H. Block Copolymer Thermodynamics: Theory and Experiment, *Annu. Rev. Phys. Chem.* **1990**, 41, 525–557.
- (15) Chen, Y.; Cui, H.; Li, L.; Tian, Z.; Tang, Z. Controlling Micro-Phase Separation in Semi-crystalline/amorphous Conjugated Block Copolymers, *Polym. Chem.* **2014**, 5, 4441–4445.
- (16) Gazit, O.; Khalfin, R.; Cohen, Y.; Tannenbaum, R. Self-Assembled Diblock Copolymer ‘Nanoreactors’ as ‘Catalysts’ for Metal Nanoparticle Synthesis, *J. Phys. Chem. C.* **2009**, 113, 576–583.
- (17) Morkved, T. L.; Lu, M.; Urbas, A. M.; Ehrichs, E. E.; Jaeger, H. M.; Mansky, P.; Russell, T. P. Local Control of Microdomain Orientation in Diblock Copolymer Thin Films with Electric Fields, *Science* **1996**, 273, 931–933.
- (18) Thurn-Albrecht, T.; Derouchey, J.; Russell, T. P.; Jaeger, H. M. Overcoming Interfacial Interactions with Electric Fields, *Macromolecules* **2000**, 33, 3250–3253.
- (19) Kim, G.; Libera, M. Morphological Development in Solvent-Cast Polystyrene - Polybutadiene - Polystyrene (SBS) Triblock Copolymer Thin Films, *Macromolecules* **1998**, 31, 2569-2577.

- (20) Kim, S. H.; Misner, M. J.; Xu, T.; Kimura, M.; Russell, T. P. Highly Oriented and Ordered Arrays from Block Copolymers via Solvent Evaporation, *Adv. Mater.* **2004**, 16, 226–231.
- (21) Rider, D. A.; Liu, K.; Eloi, J.; Vanderark, L.; Yang, L.; Wang, J.; Grozea, D.; Lu, Z.; Russell, T. P.; Manners, I. Nanostructured Magnetic Thin Films from Organometallic Block Copolymers: Pyrolysis of Self-Assembled Polystyrene-block poly(ferrocenylethylmethylsilane), *ACS Nano* **2008**, 2, 263–270.
- (22) Son, J. G.; Gwyther, J.; Chang, J. B.; Berggren, K. K.; Manners, I.; Ross, C. A. Highly Ordered Square Arrays from a Templated ABC Triblock Terpolymer, *Nano Lett.* **2011**, 11, 2849–2855.
- (23) Kim, S. O.; Solak, H. H.; Stoykovich, M. P.; Ferrier, N. J.; De Pablo, J. J.; Nealey, P. F. Epitaxial Self-assembly of Block Copolymers on Lithographically Defined Nanopatterned Substrates, *Nature* **2003**, 424, 411–414.
- (24) Bodycomb, J.; Funaki, Y.; Kimishima, K.; Hashimoto, T. Single-Grain Lamellar Microdomain from a Diblock Copolymer, *Macromolecules* **1999**, 32, 2075–2077.
- (25) Angelescu, D. E.; Waller, J. H.; Adamson, D. H.; Deshpande, P.; Chou, S. Y.; Register, R. A.; Chaikin, P. M. Macroscopic Orientation of Block Copolymer Cylinders in Single-Layer Films by Shearing, *Adv. Mater.* **2004**, 16, 1736–1740.
- (26) Singh, G.; Yager, K. G.; Berry, B.; Kim H. C.; Karim, A. Dynamic Thermal Field-Induced Gradient Soft-Shear for Highly Oriented Block Copolymer Thin Films, *ACS Nano* **2012**, 6, 10335–10342
- (27) Qiang, Z.; Zhang, L. H.; Stein, G. E.; Cavicchi, K. A.; Vogt, B. D. Unidirectional Alignment of Block Copolymer Films Induced by Expansion of a Permeable

- Elastomer during Solvent Vapor Annealing, *Macromolecules* **2014**, 47, 1109-1116.
- (28) Davis, R. L.; Chaikin, P. M.; Register, R. A. Cylinder Orientation and Shear Alignment in Thin Films of Polystyrene-Poly(n-hexyl methacrylate) Diblock Copolymers, *Macromolecules* **2014**, 47, 5277-5285.
- (29) Davis, R. L.; Michal, B. T.; Chaikin, P. M.; Register, R. A. Progression of Alignment in Thin Films of Cylinder-Forming Block Copolymers Upon Shearing, *Macromolecules* **2015**, 48, 5339-5347.
- (30) Hamada, E.; Kaneko, R. Micro-Tribological Evaluations of a Polymer Surface by Atomic Force Microscopes, *Ultramicroscopy* **1992**, 44, 184–190.
- (31) Pickering, J.; Vancso, G. On the Formation of Oriented Nanometer Scale Patterns on Amorphous Polymer Surfaces Studied by Atomic Force Microscopy, *Appl. Surf. Sci.* **1999**, 148, 147–154.
- (32) Leach, R. N.; Stevens, F.; Seiler, C.; Langford, S. C.; Dickinson, J. T. Nanometer-Scale Solvent-Assisted Modification of Polymer Surfaces Using the Atomic Force Microscope, *Langmuir* **2003**, 19, 10225–10232.
- (33) Gotsmann, B.; Dürig, U. Thermally Activated Nanowear Modes of a Polymer Surface Induced by a Heated Tip, *Langmuir* **2004**, 20, 1495–1500.
- (34) Schönherr, H.; Waymouth, R. M.; Frank, C. W. Nucleation and Crystallization of Low-Crystallinity Polypropylene Followed in Situ by Hot Stage Atomic Force Microscopy, *Macromolecules* **2003**, 36, 2412–2418.
- (35) Felts, J. R.; Onses, M. S.; Rogers, J. a; King, W. P. Nanometer Scale Alignment of Block-Copolymer Domains by Means of a Scanning Probe Tip, *Adv. Mater.* **2014**, 26,

- 2999–3002.
- (36) Leung, O. M.; Goh, M. C. Orientational Ordering of Polymers by Atomic Force Microscope Tip-Surface Interaction, *Science* **1992**, 255, 64–66.
- (37) Schmidt, R. H.; Haugstad, G.; Gladfelter, W. L. Scan-Induced Patterning and the Glass Transition in Polymer Films: Temperature and Rate Dependence of Plastic Deformation at the Nanometer Length Scale, *Langmuir* **2003**, 19, 10390–10398.
- (38) Hobbs, J. K.; Farrance, O. E.; Kailas, L. How Atomic Force Microscopy Has Contributed to Our Understanding of Polymer Crystallization, *Polymer* **2009**, 50, 4281–4292.
- (39) Harrison, C.; Adamson, D. H.; Cheng, Z.; Sebastian, J. M.; Sethuraman, S.; Huse, D. A.; Register, R. A.; Chaikin, P. M. Mechanisms of Ordering in Striped Patterns, *Science* **2000**, 290, 1558–1560.
- (40) Darko, C.; Botiz, I.; Reiter, G.; Breiby, D. W.; Andreassen, J. W.; Roth, S.V.; Smilgies, D. M.; Metwalli, E.; Papadakis, C.M. Crystallization in Diblock Copolymer Thin Films at Different Degrees of Supercooling, *Phys. Rev. E* **2009**, 79, 041802.
- (41) Vasilev, C.; Reiter, G.; Pispas, S.; Hadjichristidis, N. Crystallization of Block Copolymers in Restricted Cylindrical Geometries, *Polymer* **2006**, 47, 330–340.
- (42) Reiter, G.; Castelein, G.; Sommer, J. U.; Röttele, A.; Thurn-Albrecht, T. Direct Visualization of Random Crystallization and Melting in Arrays of Nanometer-Size Polymer Crystals, *Phys. Rev. Lett.* **2001**, 87, 226101.
- (43) Rodríguez, T. R.; García, R. Theory of Q Control in Atomic Force Microscopy, *Appl. Phys. Lett.* **2003**, 82, 4821–4823.
- (44) Hobbs, J. K.; Register, R. A. Imaging Block Copolymer Crystallization in Real Time

with the Atomic Force Microscope, *Macromolecules* **2006**, 39, 703–710.

For Table of Contents use only.

